Pramana – J. Phys. (2020) 94:104
https://doi.org/10.1007/s12043-020-01979-w

A comprehensive theoretical analysis of ^{12}B + ^{58}Ni elastic scattering measured for the first time by using different density distributions, different nuclear potentials and different cluster approaches

M AYGUN

Department of Physics, Bitlis Eren University, 13000 Bitlis, Turkey
E-mail: murata.25@gmail.com

MS received 21 October 2019; revised 28 January 2020; accepted 23 April 2020

Abstract. Recently, Zevallos *et al* [*Phys. Rev. C* **99**, 064613 (2019)] measured, for the first time, the elastic scattering data of ^{12}B + ^{58}Ni reaction at $E_{\rm Lab}$ = 30.0 and 33.0 MeV. For the first time, we show a comprehensive theoretical analysis of the experimental data of ^{12}B+^{58}Ni reaction. First, we propose alternative density distributions for the ^{12}B nucleus, and obtain the elastic scattering angular distributions of ^{12}B + ^{58}Ni reaction with the help of these densities. Secondly, we calculate the elastic scattering cross-sections of ^{12}B + ^{58}Ni reaction by using 13 different nuclear potentials to reveal alternative nuclear potentials. Finally, we examine cluster structures such as $\alpha + {}^{8}$Li and $n + {}^{11}$B of the ^{12}B nucleus by using a simple approach, and acquire elastic scattering cross-sections of ^{12}B + ^{58}Ni reaction over these cluster approaches. We compare all the theoretical results with the experimental data, and discuss their similarities and differences. Also, we propose new equations of both normalisation constant and imaginary potential parameters for all the systems analysed.

Keywords. Nuclear potential; proximity potential; cluster model; elastic scattering; optical model; double folding model.

PACS Nos 24.10.Ht; 25.70.–z

1. Introduction

Boron has 15 different isotopes from ^{7}B to ^{21}B [1,2]. The ^{10}B and ^{11}B nuclei are stable isotopes and others have short half-life. ^{12}B is the isotope with second longest half-lived nucleus with $T_{1/2}$ = 20.2 ms. Spin and parity of the ^{12}B nucleus is $I^{\pi} = 1^{+}$ [3]. ^{12}B decays into another nuclei via β^{-} and α. The ^{12}B nucleus can be obtained via ^{11}B(d,p)^{12}B reaction, for example at $E_{\rm d}$ = 1.5 MeV [4]. Also, the quadrupole moment (Q) of the ^{12}B nucleus is found to be 13.21 ± 0.26 mb [4].

Recently, Zevallos *et al* [5] have measured, for the first time, the elastic scattering cross-sections of ^{12}B + ^{58}Ni reaction at incident energies of $E_{\rm Lab}$ = 30.0 and 33.0 MeV. They have analysed the experimental data with the help of large-scale coupled channel (CC) and coupled reaction channel (CRC) calculations. However, we think that developing theoretical knowledge to explain experimental data of ^{12}B + ^{58}Ni reaction by using different approaches will be useful in describing the subsequent ^{12}B reactions.

The density distribution is one of the most important inputs in determining elastic scattering cross-sections of the nuclei [6–13]. In this sense, alternative density distributions of the nuclei can be found in [14]. However, the determination of ideal density distribution is still one of the hottest topics in the field of nuclear physics. When the density distributions related to ^{12}B nucleus are examined, it can be seen that there are not many alternatives in the literature. As a result, it is inevitable to obtain alternative density distributions of the ^{12}B nucleus whose experimental data have been measured for the first time.

Another important point in the analysis of elastic scattering cross-sections is to get appropriate nuclear potential. Thus, suitable theoretical results will be achieved for the analysed experimental data. In order to evaluate nuclear interactions of the ^{12}B nucleus, different nuclear

Published online: 16 July 2020

potentials will be investigated in our study, and alternative potentials will be put forward.

Cluster structure is an important tool to characterise the structure of nuclei. For this purpose, different approaches have been performed. The Bloch–Brink α-cluster model (ACM), the antisymmetrised molecular dynamics (AMD) and the generator coordinate method (GCM) are some of them [15]. In recent years, Aygun examined ^{9}Li [16], ^{9}Be [17] and ^{12}Be [18] nuclei by using a simple cluster method. We think it would be useful to analyse $\alpha + {}^{8}$Li and $n + {}^{11}$B cluster structures of the ^{12}B nucleus using this simple approach.

In this study, we introduce three different approaches to explain the elastic scattering cross-sections of ^{12}B + ^{58}Ni reaction at incident energies of $E_{\mathrm{Lab}} = 30.0$ and 33.0 MeV. First, we produce alternative density distributions for the ^{12}B nucleus in different models. We obtain elastic scattering angular distributions of ^{12}B + ^{58}Ni reaction over these density distributions. We determine appropriate density distribution by comparing the results with each other and with experimental data.

Secondly, to put forward alternative nuclear potentials, we calculate elastic scattering angular distributions of ^{12}B + ^{58}Ni reaction by using 13 different nuclear potentials consisting of proximity 1977, modified proximity 1988, proximity 1995, proximity 2003-I, proximity 2003-II, proximity 2003-III, proximity 2010, Broglia and Winther 1991, Aage Winther, Bass 1980, Christensen and Winther 1976, Ngo 1980 and Denisov. We show useful potentials over the theoretical results.

Finally, to obtain alternative computational paths for the theoretical analysis of the nuclear interactions with the ^{12}B nucleus, we examine the cluster structures of the ^{12}B nucleus using a different approach. We obtain elastic scattering cross-sections of ^{12}B + ^{58}Ni reaction for $\alpha + {}^{8}$Li and $n + {}^{11}$B cluster structures of the ^{12}B nucleus by using a simple approach. We compare all theoretical results with experimental data, and discuss similarities and differences of the theoretical results.

The next section shows the calculation formalism. Section 3 gives the density distributions of the projectile and the target nuclei. Section 4 provides the nuclear potentials used in the calculations. Section 5 presents an alternative approach for the cluster structure of the ^{12}B nucleus. Section 6 demonstrates the results and discussion. Section 7 gives the summary and conclusions.

2. Calculation formalism

2.1 *Optical model*

In the theoretical calculations with the optical model, we can choose the effective potential as the sum of Coulomb and nuclear potentials as follows:

$$V_{\mathrm{Total}}(r) = V_{\mathrm{Coulomb}}(r) + \underbrace{V_{\mathrm{Nuclear}}(r)}_{\underbrace{V(r)}_{\text{Real Part}} + \underbrace{iW(r)}_{\text{Imaginary Part}}}, \tag{1}$$

where the Coulomb potential [19] is

$$V_{\mathrm{Coulomb}}(r) = \frac{1}{4\pi\epsilon_{\circ}}\frac{Z_P Z_T e^2}{r}, \quad r \geq R_c \tag{2}$$

$$V_{\mathrm{Coulomb}}(r) = \frac{1}{4\pi\epsilon_{\circ}}\frac{Z_P Z_T e^2}{2R_c}\left(3 - \frac{r^2}{R_c^2}\right), \quad r < R_c \tag{3}$$

$$R_c = 1.25(A_P^{1/3} + A_T^{1/3}), \tag{4}$$

where R_c is the Coulomb radius, $Z_P(Z_T)$ denotes the charge of the projectile(target) nucleus and $A_P(A_T)$ is the mass number of the projectile(target) nucleus, respectively.

The choice of nuclear potential is very important in explaining nuclear interactions. In this context, the nuclear potential part of the optical model consists of real and imaginary potentials. To obtain the real potential, three different approaches comprising different density distributions, different nuclear potentials, and different cluster structures are used in our study. The theoretical information about the approaches is given in the subsections.

The other potential for the optical model is its imaginary part. The imaginary potential to be used for this purpose in our study is the Woods–Saxon potential in the following form:

$$W(r) = -\frac{W_0}{1 + \exp\left(\frac{r - R_w}{a_w}\right)}, \quad R_w = r_w(A_P^{1/3} + A_T^{1/3}), \tag{5}$$

where W_0, r_w and a_w are the depth, radius and diffuseness parameter. The code FRESCO [20] is used in the calculations.

2.2 *Double folding model*

The double folding model is an efficient model commonly used to produce the real potential of the optical model. The double folding potential applicable for this purpose can be written as

$$V(\vec{r}) = \int \mathrm{d}\vec{r}_1 \int \mathrm{d}\vec{r}_2 \rho_P(\vec{r}_1)\rho_T(\vec{r}_2)v_{NN}(\vec{r} - \vec{r}_1 + \vec{r}_2), \tag{6}$$

where $\rho_{P(T)}(\vec{r}_{1(2)})$ are the density distributions of the projectile and the target nuclei, respectively, and v_{NN} is

the nucleon–nucleon interaction parameterised by [19]

$$v_{NN}(r) = 7999\,\frac{\exp(-4r)}{4r} - 2134\,\frac{\exp(-2.5r)}{2.5r} + 276\left(1 - 0.005\frac{E_{\rm Lab}}{A_p}\right)\delta(r)\ \text{MeV}. \quad (7)$$

The density distribution of the projectile and the target nuclei play a very important role in achieving double folding potential. Therefore, determining the density distribution appropriate to the nuclei is an important input in obtaining nuclear potential compatible with experimental data.

3. Density distributions

One of the first stages of the present work is to examine the density distributions of the ^{12}B nucleus. For this, eight different density distributions of ^{12}B are evaluated to obtain the real part of the optical model potential. The density distributions of the projectile (^{12}B) and the target (^{58}Ni) nuclei are given in Appendix A.

4. Nuclear potentials

In the theoretical analysis of elastic scattering cross-sections of ^{12}B + ^{58}Ni reaction, we apply 13 different nuclear potentials to get the real part of the optical model. The potentials are summarised in Appendix B.

5. Simple cluster approach

The cluster structure is an important approach to examine the structural properties of nuclei. Different methods have been proposed for this purpose. Recently, Aygun investigated ^{9}Li [16], ^{9}Be [17] and ^{12}Be [18] nuclei by using the simple cluster method. In the present work, we apply the simple cluster approach to determine the elastic scattering cross-sections of the ^{12}B nucleus. With this goal, we examine $\alpha + {}^{8}$Li and $n + {}^{11}$B cluster cases known for ^{12}B projectile in the literature.

5.1 $\alpha + {}^{8}$*Li cluster structure*

The ^{12}B nucleus can be evaluated as α + ^{8}Li cluster structure [21,22]. In this manner, ^{12}B density can be assumed as the sum of the density distributions of α and ^{8}Li given by

$$\rho_{^{12}\rm B}(r) = \rho_{\alpha}(r) + \rho_{^{8}\rm Li}(r). \quad (8)$$

α density distribution is taken in Gaussian form [23]

$$\rho_{\alpha}(r) = 0.4229\,\exp(-0.7024r^2). \quad (9)$$

^{8}Li density is considered as [24]

$$\rho_{c}(r) = \left(\frac{3}{2\pi R_c^2}\right)^{3/2}\exp\left(-\frac{3r^2}{2R_c^2}\right), \quad (10)$$

$$\rho_{v}(r) = \left(\frac{3}{2\pi R_v^2}\right)^{3/2}\exp\left(-\frac{3r^2}{2R_v^2}\right), \quad (11)$$

where R_c and R_v are 2.50 fm and 2.53 fm, respectively [25]. The total matter distribution ρ_m, normalised to unity [24], is formulated by

$$\rho_m(r) = [N_c\rho_c(r) + (A - N_c)\rho_v(r)]/A, \quad (12)$$

where N_c and A are the number of nucleons in the core and the mass number, respectively.

5.2 $n + {}^{11}B$ *cluster structure*

The ^{12}B nucleus can also be a cluster form such as n + ^{11}B [22]. Thus, ^{12}B density distribution can be written as

$$\rho_{^{12}\rm B}(r) = \rho_{\rm n}(r) + \rho_{^{11}\rm B}(r). \quad (13)$$

^{11}B density is evaluated as [26]

$$\rho_{^{11}\rm B}(r) = (0.18465{+}0.052432r^2)\exp(-0.350133r^2). \quad (14)$$

The neutron density is taken in the Gaussian form given by [27,28]

$$\rho_{\rm n}(r) = \left(\frac{1}{\gamma\sqrt{\pi}}\right)^{3}\exp(-r^2/\gamma^2), \quad (15)$$

where γ is adjusted to reproduce the experimental value for the root mean square (rms) radius of ^{12}B.

6. Results and discussion

6.1 *Analysis with different density distributions*

One of the aims of our study is to propose alternative density distributions for the ^{12}B nucleus whose experimental data have been measured for the first time. Then, the most suitable density distribution with the experimental data is to be determined over the analysed densities. The rms values of the density distributions are given in table 1.

In the present work, eight different density distributions for the ^{12}B nucleus are given, which are called as SP, 2pF, Ngo, G1, G2, W, S and M. The theoretical calculations were based on the optical model. In this context, the real part of the optical model potential

Table 1. The rms radii for the SP, 2pF, Ngo, G1, G2, W, S and M density distributions.

Nucleus	SP	2pF	Ngo	G1	G2	W	S	M	Literature
^{12}B	2.347	2.592	2.667	2.331	2.311	2.353	2.725	2.759	2.33[a], 3.16 ± 0.32[b]

[a]Determined with the Gaussian–Gaussian function distribution [29].
[b]Determined via ref. [30].

was calculated for eight density distributions by using double folding model calculations which is presented in Sect. 2.2. In the double folding model calculations, the code DFPOT [31] was used. The imaginary part of the optical model potential was the Woods–Saxon-type potential. To achieve good agreement with the experimental data, the parameters (W_0, r_w and a_w) of the imaginary potential were studied at 0.1 and 0.01 step intervals. The global equations of these parameters were obtained for the values giving the theoretical cross-sections, and are listed in table 2. In the optical model calculations, the code FRESCO [20] was applied.

Figure 1 presents the changes with r of eight different density distributions of the ^{12}B nucleus. It is seen from figure 1a that W density gives the highest density distribution in the centre part, whereas 2pF density has the lowest density distribution in the centre. Also, one can see that SP, G1, G2 and W density distributions in the centre are greater than the assumed value of nuclear saturation density, especially for W density. On the other hand, 2pF, Ngo, S and M densities are around nuclear saturation. The rms value is a parameter that shows the measure of the size of a nucleus. It can be seen that the rms values of SP, G1, G2 and W density distributions are slightly smaller than the rms values of other density distributions when the rms values calculated for eight different density distributions are examined (table 1). It may be said that the they are more concentrated in the centre. However, figure 1b displays the tails of the densities between 4 and 6 fm in logarithmic scale. It is seen from figure 1b that some densities, which are different in the centre part, show similar tails. In this context, the behaviours of Ngo and S densities have been observed to be very similar. Moreover, SP, G1 and G2 density distributions are seen to be very close to each other between 5 and 6 fm. A similar situation can be seen for Ngo, S and M density distributions.

Figure 2 shows the elastic scattering angular distributions of ^{12}B projectile by ^{58}Ni target nucleus at an incident energy of 30 MeV. It is observed that all density distributions are quite successful in explaining experimental data. Additionally, it can be stated that the results of G1 and G2 density distributions are very close to each other, and are slightly better than the results of other densities.

Figure 3 provides the elastic scattering cross-sections of $^{12}\mathrm{B} + {}^{58}\mathrm{Ni}$ reaction for eight different densities at 33 MeV. The results are also compared with the experimental data. It is found that SP and G1 density distributions are quite successful in explaining the forward angles of the experimental data while they have failed in determining the Fresnel diffraction which is observed in the experimental data. On the other hand, it is seen that Ngo, S and M densities are successful in explaining the behaviour of the Fresnel diffraction while they are poor in producing the forward angles of the experimental data.

Figure 4 shows the real potentials of SP, 2pF, Ngo, G1, G2, W, S and M density distributions. It can be seen that SP, G1, G2 and W density distributions have demonstrated similar features. We can observe that G2 density distribution is deeper than the other density distributions at both 30 and 33 MeV. It is also noticed that the order of the depths of the density distributions is similar at both energy values.

6.2 *Analysis with different nuclear potentials*

It is important to offer an appropriate potential for $^{12}\mathrm{B} + {}^{58}\mathrm{Ni}$ reaction to explain both $^{12}\mathrm{B} + {}^{58}\mathrm{Ni}$ and other ^{12}B-nucleus reactions. With this goal, we have investigated 13 different potentials such as Prox 77, Mod-Prox 88, Prox 95, Prox 2003-I, Prox 2003-II, Prox 2003-III, Prox 2010, BW 91, AW 95, Bass 80, CW 76, Ngo 80 and D. The changes as a function of distance (r) of these potentials are presented in figure 5.

The theoretical calculations with different nuclear potentials were carried out under the optical model. In this respect, proximity potentials were first obtained using FORTRAN code which is written by us. Then, the FRESCO code for the resulting values were generated. The imaginary part of the optical model potential was taken as Woods–Saxon-type potential. The parameters of the imaginary potential were examined at 0.1 and 0.01 step intervals to obtain a good harmony between the theoretical results and the experimental data. The global equations of these parameters were achieved for the values providing the theoretical cross-sections, and are shown in table 2. In the optical model calculations, the code FRESCO [20] was used.

Figure 6 displays the elastic scattering cross-sections of ^{12}B on ^{58}Ni at 30 MeV. It is observed that the results of Mod-Prox 88, Prox 95, Prox 2010, BW 91, AW 95,

Table 2. The equations of normalisation constant and imaginary potential parameters obtained from the theoretical calculations of $^{12}B + ^{58}Ni$ reaction by using SP, 2pF, Ngo, G1, G2, W, S and M density distributions, Prox 77, Mod-Prox 88, Prox 95, Prox 2003-I, Prox 2003-II, Prox 2003-III, Prox 2010, BW 91, AW 95, Bass 80, CW 76, Ngo 80, D potentials, and $\alpha + ^{8}Li$ and $n + ^{11}B$ cluster states.

System	N_R	W_0	r_w	a_w
SP	$8.93 - 0.26000E_{Lab}$,	$19.1 - 0.03333E_{Lab}$,	$1.26 + 0.00001E_{Lab}$,	$0.25 + 0.00667E_{Lab}$
2pF	$6.68 - 0.19333E_{Lab}$,	$98.5 - 2.66667E_{Lab}$,	$1.26 + 0.00001E_{Lab}$,	$0.54 + 0.00001E_{Lab}$
Ngo	$5.03 - 0.14333E_{Lab}$,	$42.5 - 0.83333E_{Lab}$,	$1.26 + 0.00001E_{Lab}$,	$1.34 + 0.02667E_{Lab}$
G1	$9.24 - 0.27000E_{Lab}$,	$60.5 - 1.53333E_{Lab}$,	$1.27 + 0.00001E_{Lab}$,	$0.55 - 0.00001E_{Lab}$
G2	$8.38 - 0.24000E_{Lab}$,	$3.50 + 0.33333E_{Lab}$,	$1.16 + 0.00333E_{Lab}$,	$1.67 - 0.03667E_{Lab}$
W	$10.2 - 0.30000E_{Lab}$,	$37.5 - 0.66667E_{Lab}$,	$1.25 + 0.00001E_{Lab}$,	$1.07 - 0.01667E_{Lab}$
S	$4.70 - 0.13333E_{Lab}$,	$19.1 - 0.06667E_{Lab}$,	$1.26 + 0.00001E_{Lab}$,	$1.54 - 0.03333E_{Lab}$
M	$4.70 - 0.13333E_{Lab}$,	$7.90 + 0.36667E_{Lab}$,	$1.24 + 0.00001E_{Lab}$,	$1.56 - 0.03333E_{Lab}$
Prox 77	$4.30 - 0.11000E_{Lab}$,	$52.0 - 1.00000E_{Lab}$,	$1.26 + 0.00001E_{Lab}$,	$1.88 - 0.04333E_{Lab}$
Mod-Prox 88	$7.00 - 0.20000E_{Lab}$,	$-34.3 + 1.60000E_{Lab}$,	$1.26 + 0.00001E_{Lab}$,	$1.88 - 0.04333E_{Lab}$
Prox 95	$8.75 - 0.25000E_{Lab}$,	$-31.7 + 1.53333E_{Lab}$,	$1.26 + 0.00001E_{Lab}$,	$1.88 - 0.04333E_{Lab}$
Prox 2003-I	$6.52 - 0.18000E_{Lab}$,	$3.50 + 0.46667E_{Lab}$,	$1.26 + 0.00001E_{Lab}$,	$1.88 - 0.04333E_{Lab}$
Prox 2003-II	$5.62 - 0.15000E_{Lab}$,	$40.0 - 0.63333E_{Lab}$,	$1.26 + 0.00001E_{Lab}$,	$1.88 - 0.04333E_{Lab}$
Prox 2003-III	$5.30 - 0.14000E_{Lab}$,	$38.8 - 0.60000E_{Lab}$,	$1.26 + 0.00001E_{Lab}$,	$1.88 - 0.04333E_{Lab}$
Prox 2010	$8.03 - 0.23000E_{Lab}$,	$-46.0 + 1.96667E_{Lab}$,	$1.26 + 0.00001E_{Lab}$,	$1.88 - 0.04333E_{Lab}$
BW 91	$9.01 - 0.26000E_{Lab}$,	$-47.2 + 2.00000E_{Lab}$,	$1.26 + 0.00001E_{Lab}$,	$1.78 - 0.04000E_{Lab}$
AW 95	$7.93 - 0.22667E_{Lab}$,	$21.9 - 0.30000E_{Lab}$,	$1.26 + 0.00001E_{Lab}$,	$1.38 - 0.02667E_{Lab}$
Bass 80	$7.94 - 0.23000E_{Lab}$,	$5.20 + 0.26667E_{Lab}$,	$1.16 + 0.00333E_{Lab}$,	$1.48 - 0.03000E_{Lab}$
CW 76	$8.47 - 0.24333E_{Lab}$,	$-42.0 + 1.83333E_{Lab}$,	$1.26 + 0.00001E_{Lab}$,	$1.98 - 0.04667E_{Lab}$
Ngo 80	$3.40 - 0.08000E_{Lab}$,	$150.0 - 4.00000E_{Lab}$,	$1.26 + 0.00001E_{Lab}$,	$1.38 - 0.02667E_{Lab}$
D	$1.00 - 0.00001E_{Lab}$,	$-32.0 + 1.50000E_{Lab}$,	$2.25 - 0.03000E_{Lab}$,	$0.88 - 0.01000E_{Lab}$
$\alpha + ^{8}Li$	$7.76 - 0.22000E_{Lab}$,	$-9.00 + 0.66667E_{Lab}$,	$1.42 - 0.00333E_{Lab}$,	$1.61 - 0.03667E_{Lab}$
$n + ^{11}B$	$4.15 - 0.11667E_{Lab}$,	$10.0 + 0.00001E_{Lab}$,	$1.42 - 0.00333E_{Lab}$,	$1.51 - 0.03333E_{Lab}$

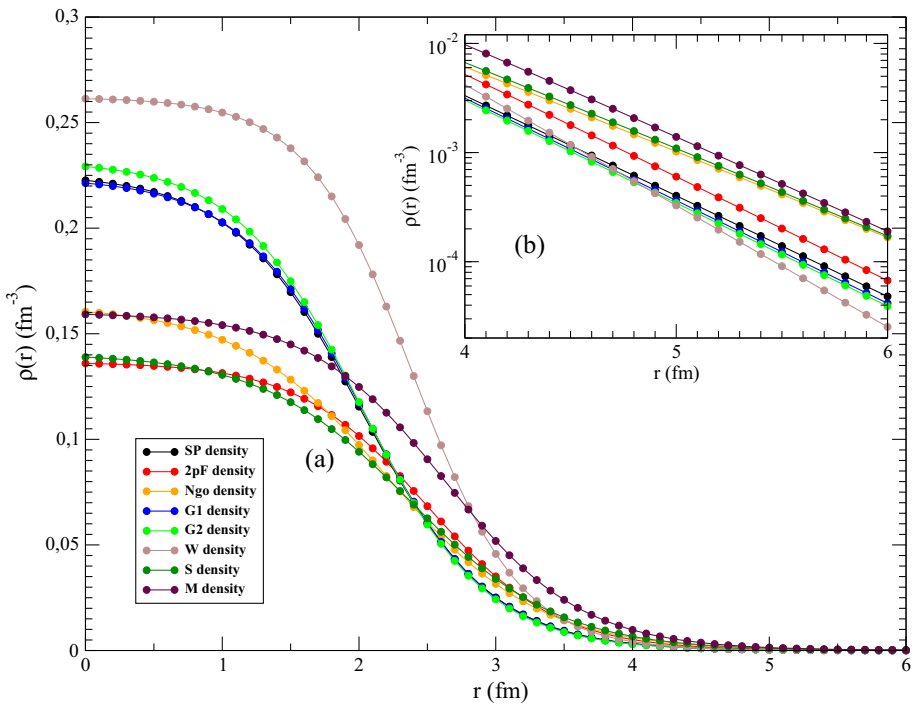

Figure 1. (**a**) SP, 2pF, Ngo, G1, G2, W, S and M density distributions of the ^{12}B nucleus in linear scale and (**b**) the tails of densities between 4 and 6 fm in logarithmic scale.

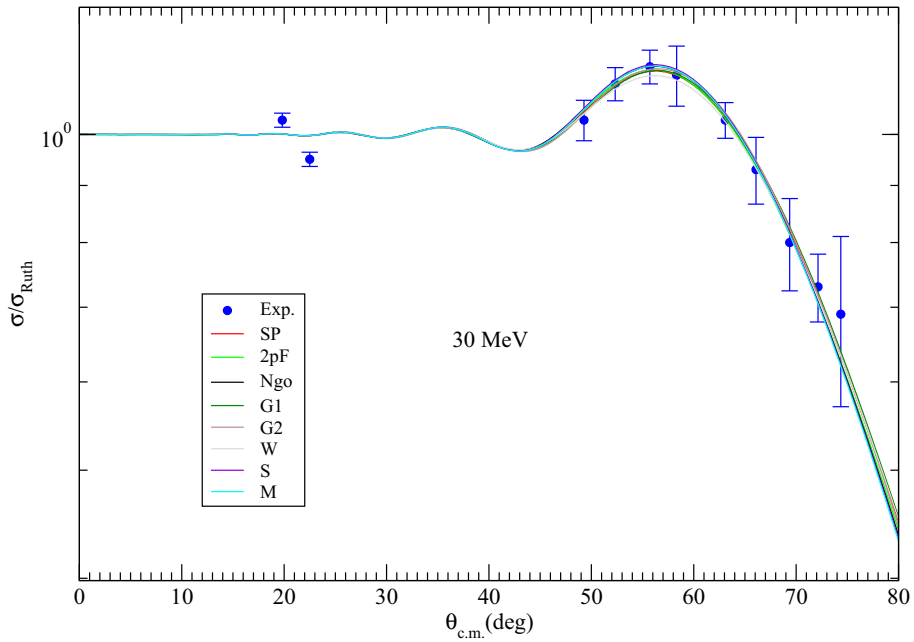

Figure 2. The elastic scattering cross-sections of ^{12}B + ^{58}Ni reaction calculated using SP, 2pF, Ngo, G1, G2, W, S and M density distributions in comparison with the experimental data at $E_{\text{Lab}} = 30$ MeV. The experimental data are taken from ref. [32].

Bass 80 and CW 76 potentials are very close to each other. These potentials are also quite good in defining both Fresnel diffraction and experimental data. On the other hand, it has been realised that the results of Prox 77, Prox 2003-I, Prox 2003-II, Prox 2003-III, Ngo 80 and D potentials are insufficient to define both Fresnel diffraction and experimental data.

Figure 7 shows the elastic scattering results of ^{12}B + ^{58}Ni reaction at 33 MeV. It is seen that the results of Prox 77, Mod-Prox 88, Prox 95, Prox 2003-I, Prox 2003-II, Prox 2003-III potentials are very close to each other. These potentials are better than the other potential results in defining both Fresnel diffraction and experimental data. However, the most incompatible results with experimental data have appeared for the D potential.

6.3 *Analysis with simple cluster approach*

In this section, we have examined the cluster states known for the ^{12}B nucleus in the literature by using a simple approach. For this, we have analysed $\alpha + {}^{8}$Li and $n + {}^{11}$B cluster structures of ^{12}B. The calculations with simple cluster approach were performed within the optical model. The cluster calculations are similar to the calculations of the density distributions given in Sect. 6.1. In this respect, the real part of the optical model potential was obtained for two different cluster states of ^{12}B within the double folding model by using the code DFPOT [31]. The imaginary part of the optical model potential was assumed to be Woods–Saxon-type potential. The parameters of the imaginary potential were studied at 0.1 and 0.01 step intervals. The global equations of these parameters were obtained for the values giving the theoretical results, and are displayed in table 2. In the optical model calculations, the code FRESCO [20] was used.

Figure 8 presents the elastic scattering cross-sections of ^{12}B + ^{58}Ni reaction at 30 and 33 MeV. We have observed that the result of $\alpha + {}^{8}$Li cluster state is better than $n + {}^{11}$B at 30 MeV. At 33 MeV, it is noticed that the theoretical results of $\alpha + {}^{8}$Li and $n + {}^{11}$B cluster cases are very similar to each other, and the compatibility with experimental data is quite good.

The normalisation constant (N_R) is used to increase the agreement between the experimental data and the theoretical calculations. In this sense, it is accepted that $N_R \approx 1$ presents the success of the theoretical results. If N_R deviates from unity, it is thought as the uncertainty or oddity in the data or to the fitting procedure [23]. In this study, we have changed N_R in the theoretical calculations to get more agreement with the experimental data. We have used the N_R value that will yield the best matching results with the experimental data. We have noticed that the normalisation constants of both cluster structures deviate from unity. However, we have

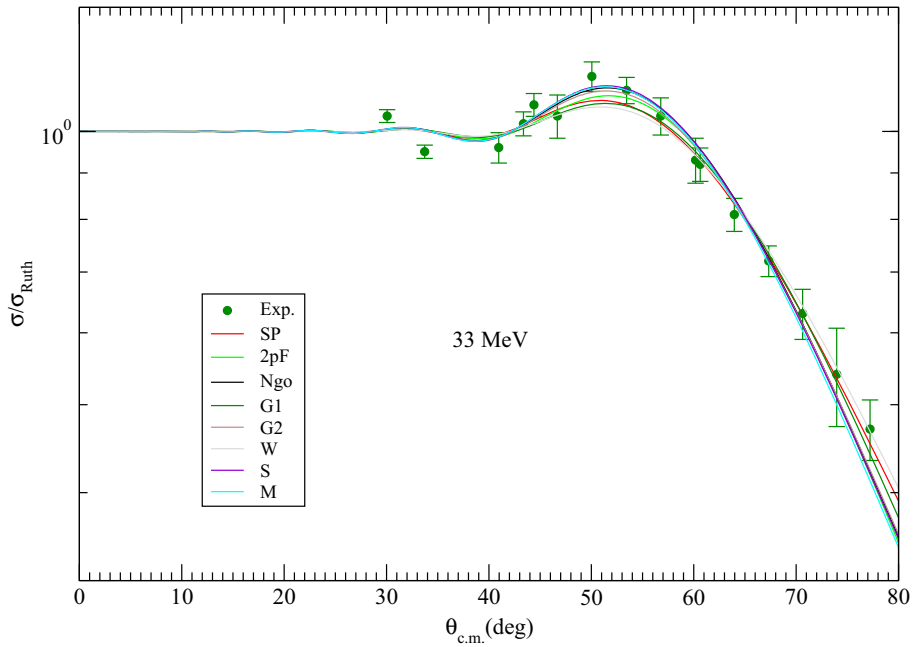

Figure 3. Same as figure 2, but for $E_{\mathrm{Lab}} = 33$ MeV. The experimental data are taken from ref. [32].

observed that the deviation in $\alpha + {}^{8}$Li cluster state is less than that of $n + {}^{11}$B cluster state. As a result, we can conclude that $\alpha + {}^{8}$Li cluster state are more efficient than $n + {}^{11}$B cluster state in terms of both theoretical results and normalisation constants. We would like to point out that the results mentioned here are not a definite case but it is intended to bring a different perspective to future studies.

6.4 *Equations of normalisation constant and imaginary potential parameters*

In the present study, the normalisation constant is changed to increase the consistency between experimental data and theoretical results with density distribution, nuclear potential and cluster approach calculations. According to the values of N_R used in the calculations, the equations that give N_R value for each case were obtained.

The imaginary part of the optical potential in the theoretical calculations of density distributions, nuclear potentials and cluster structures was assumed to be of Woods–Saxon type. The potential parameters were released to achieve good agreement with the experimental data. In this context, the potential parameters were investigated at 0.1 and 0.01 step intervals.

It is important to determine the potential parameters to be used in the analysis of nuclear reactions. For this purpose, we have acquired the equations of the normalisation constant and imaginary potential parameters for all the systems analysed in this work by evaluating the imaginary potential parameters found using the elastic scattering cross-section calculations. Thus, 92 equations obtained are given in table 2.

6.5 *Reaction cross-sections*

The cross-section is one of the main parameters in the analysis of nuclear reactions. In this context, the cross-section is an important tool for nuclear radius measurements, to reveal non-general conditions observed in nuclei or to obtain more information about optical potential of nuclear reaction analysed [33].

In our work, we have listed the cross-sections for all the analysed systems for both 30 and 33 MeV energies in table 3. We have noticed that the cross-sections are between 637 and 679 mb at 30 MeV, and between 625 and 688 mb at 33 MeV. We have observed that the cross-sections have supported each other in both energies. As a result, similar cross-section values obtained from the optical model calculations over different approaches can be attributed to the well-defined experimental data. Therefore, it can be concluded that the approaches used in our study are suitable for ^{12}B + ^{58}Ni reaction.

7. Summary and conclusions

In the present study, our aim was to propose alternative density distributions, alternative nuclear potentials and alternative cluster approach for the ^{12}B nucleus.

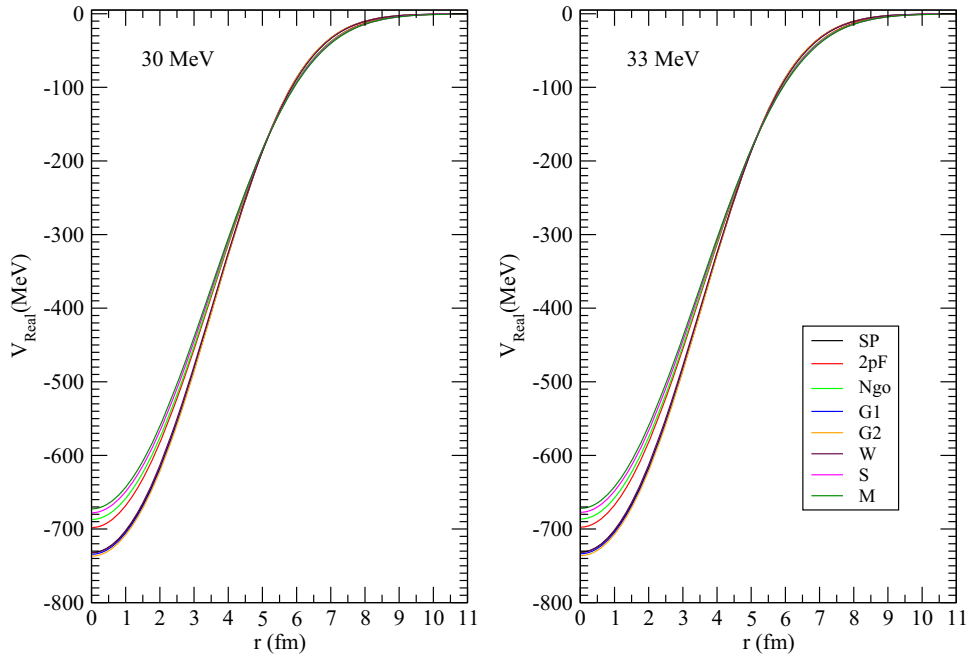

Figure 4. The shapes of the real potentials of $^{12}B + ^{58}Ni$ reaction for SP, 2pF, Ngo, G1, G2, W, S and M density distributions at $E_{Lab} = 30$ and 33 MeV.

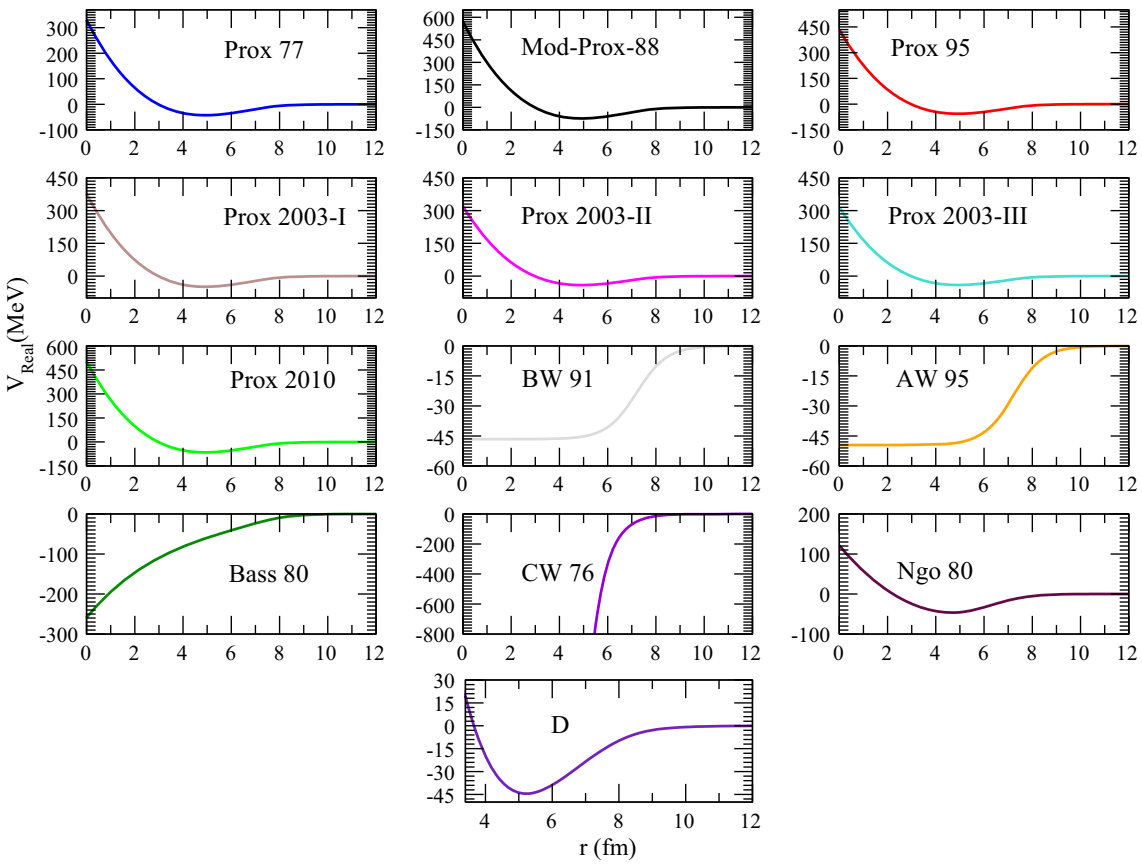

Figure 5. Distance-dependent changes of the real parts of nuclear potentials such as Prox 77, Mod-Prox 88, Prox 95, Prox 2003-I, Prox 2003-II, Prox 2003-III, Prox 2010, BW 91, AW 95, Bass 80, CW 76, Ngo 80 and D.

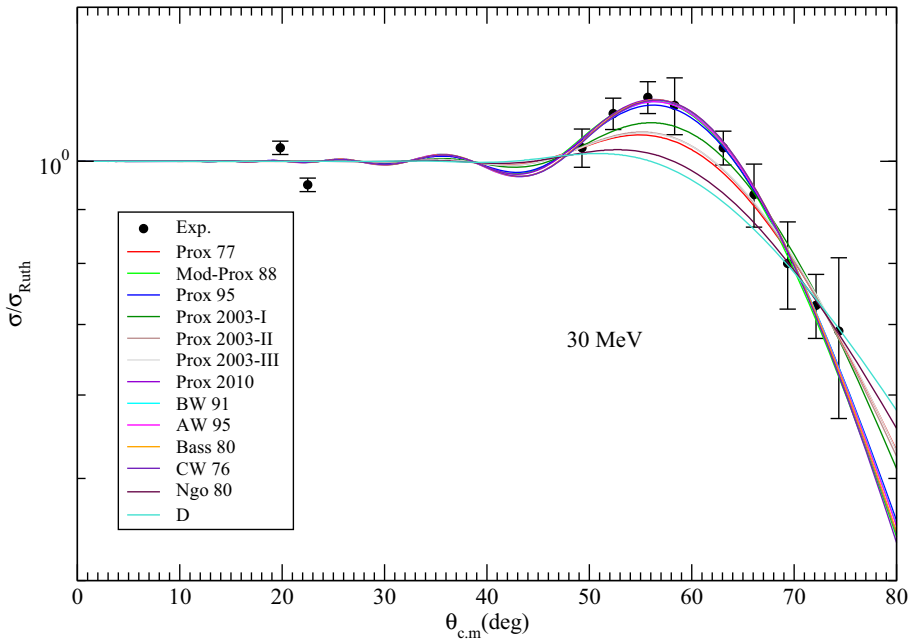

Figure 6. The elastic scattering cross-sections of $^{12}B + ^{58}Ni$ reaction calculated using Prox 77, Mod-Prox 88, Prox 95, Prox 2003-I, Prox 2003-II, Prox 2003-III, Prox 2010, BW 91, AW 95, Bass 80, CW 76, Ngo 80 and D potentials in comparison with the experimental data at $E_{Lab} = 30$ MeV. The experimental data are taken from ref. [32].

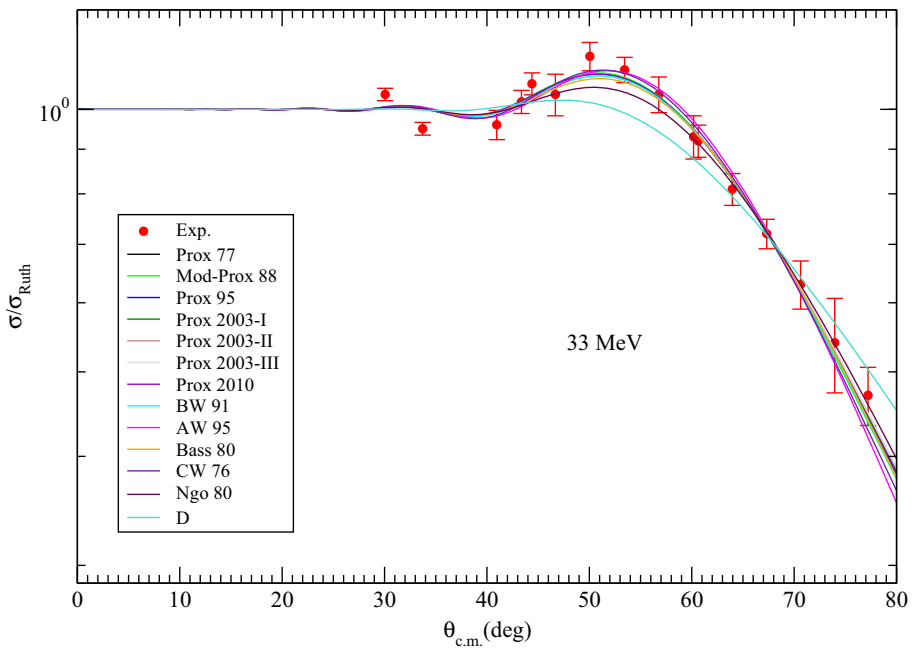

Figure 7. Same as figure 6, but for $E_{Lab} = 33$ MeV. The experimental data are taken from ref. [32].

We have calculated the elastic scattering cross-sections of $^{12}B + ^{58}Ni$ reaction by using eight different density distributions of the ^{12}B nucleus. We have compared all the theoretical results with the experimental data, and have observed that there is very good agreement between the theoretical results and the experimental data.

Then, we have investigated the elastic scattering angular distributions of $^{12}B + ^{58}Ni$ reaction for 13 different nuclear potentials. We have obtained the theoretical

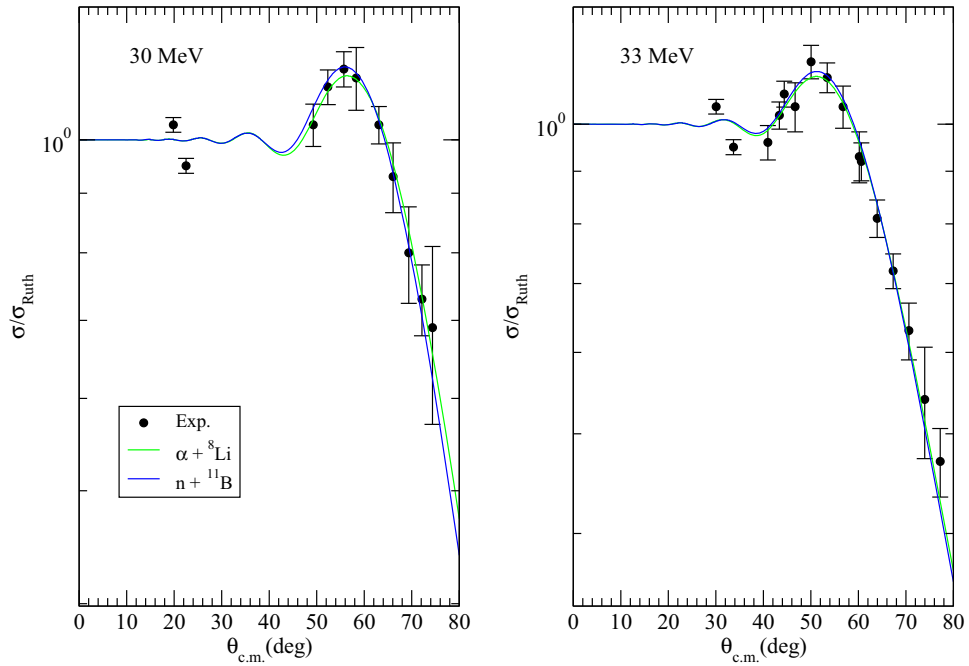

Figure 8. The elastic scattering angular distributions of $^{12}B + ^{58}Ni$ reaction calculated using $\alpha + ^{8}Li$ and $n + ^{11}B$ cluster structures of the ^{12}B nucleus. The experimental data are taken from ref. [32].

Table 3. The cross-sections (in mb) obtained for SP, 2pF, Ngo, G1, G2, W, S and M density distributions, Prox 77, Mod-Prox 88, Prox 95, Prox 2003-I, Prox 2003-II, Prox 2003-III, Prox 2010, BW 91, AW 95, Bass 80, CW 76, Ngo 80, D potentials, and $\alpha + ^{8}Li$ and $n + ^{11}B$ cluster calculations.

System	30 MeV	33 MeV
σ_{SP}	663	655
σ_{2pF}	667	671
σ_{Ngo}	659	641
σ_{G1}	659	675
σ_{G2}	662	653
σ_{W}	674	663
σ_{S}	659	637
σ_{M}	666	649
$\sigma_{Prox\ 77}$	659	643
$\sigma_{Mod\text{-}Prox\ 88}$	662	643
$\sigma_{Prox\ 95}$	658	641
$\sigma_{Prox\ 2003\text{-}I}$	650	642
$\sigma_{Prox\ 2003\text{-}II}$	659	641
$\sigma_{Prox\ 2003\text{-}III}$	655	640
$\sigma_{Prox\ 2010}$	656	642
$\sigma_{BW\ 91}$	663	658
$\sigma_{AW\ 95}$	665	659
$\sigma_{Bass\ 80}$	663	663
$\sigma_{CW\ 76}$	673	649
$\sigma_{Ngo\ 80}$	679	682
σ_{D}	667	688
$\sigma_{\alpha+^{8}Li}$	647	642
$\sigma_{n+^{11}B}$	637	625

results which are in good agreement with the experimental data. In this respect, we have noticed that Mod-Prox 88 and Prox 95 potentials have given better results than the other potentials in both energies.

Finally, we have analysed different cluster configurations of the ^{12}B nucleus by using a simple cluster method. The results obtained are in good agreement with the experimental data. Additionally, we have observed that that $\alpha + ^{8}Li$ cluster state is more efficient than $n + ^{11}B$ cluster state over theoretical results and normalisation constants.

Consequently, this study presents new and important results in explaining the experimental data of $^{12}B + ^{58}Ni$ reaction which is measured for the first time. Thus, our study also provides alternative density distributions, alternative nuclear potentials and an alternative computational approach for different cluster states of ^{12}B for the analysis of experimental data of ^{12}B-nucleus reactions. Also, we believe that this study will contribute an idea for calculations related to neighbouring nuclei with the help of density distributions, nuclear potentials and simple cluster calculations.

Acknowledgements

Author thanks the referee for valuable discussion and comments.

Appendix A: Density distributions

A.1 *Density distributions of* ^{12}B *projectile*

A.1.1 *São Paulo density distribution.* São Paulo density which has the two-parameter Fermi (2pF) shape [34] can be given by

$$\rho_i(r) = \frac{\rho_{0i}}{1+\exp\left(\frac{r-R_i}{a_i}\right)}, \quad i = n, p \tag{16}$$

$$R_n = 1.49N^{1/3} - 0.79, \quad a_n = 0.47 + 0.00046N, \tag{17}$$

$$R_p = 1.81Z^{1/3} - 1.12, \quad a_p = 0.47 - 0.00083Z, \tag{18}$$

where $R_{n(p)}$ and $a_{n(p)}$ are half-density radius and surface thickness parameter of neutron(proton), respectively. The São Paulo density is shown as SP in our study.

A.1.2 *Fermi density distribution.* Fermi density is in the same form as SP density distribution except for the values of R_n, R_p, a_n and a_p. Thus, $R_{n(p)}$ and $a_{n(p)}$ values are derived from the following equations [35]:

$$R_n = 0.953N^{1/3} + 0.015Z + 0.774,$$
$$a_n = 0.446 + 0.0072\left(\frac{N}{Z}\right), \tag{19}$$
$$R_p = 1.322Z^{1/3} + 0.007N + 0.022,$$
$$a_p = 0.449 + 0.0071\left(\frac{Z}{N}\right). \tag{20}$$

Fermi density is shown as 2pF in our work.

A.1.3 *Ngô–Ngô density distribution.* Ngô–Ngô density distribution is parametrised as [36,37]

$$\rho_i(r) = \frac{\rho_{0i}}{1+\exp\left(\frac{r-C_i}{0.55}\right)}, \quad i = n, p \tag{21}$$

$$\rho_{0n} = \frac{3}{4\pi}\frac{N}{A}\frac{1}{r_{0n}^3}, \quad \rho_{0p} = \frac{3}{4\pi}\frac{Z}{A}\frac{1}{r_{0p}^3}, \tag{22}$$

where C, the central radius, is

$$C = R\left(1 - \frac{1}{R^2}\right), \quad R = \frac{NR_n + ZR_p}{A}. \tag{23}$$

The sharp radii of neutron and proton are formulated by

$$R_n = r_{0n}A^{1/3}, \quad r_{0n} = 1.1375 + 1.875 \times 10^{-4}A, \tag{24}$$

$$R_p = r_{0p}A^{1/3}, \quad r_{0p} = 1.128 \text{ fm}. \tag{25}$$

Ngô–Ngô density is shown as Ngo in our study.

A.1.4 *Gupta density distribution* 1. Gupta density distribution is shown as

$$\rho_i(r) = \frac{\rho_{0i}}{1+\exp\left(\frac{r-R_{0i}}{a_i}\right)},$$
$$\rho_{0i} = \frac{3A_i}{4\pi R_{0i}^3}\left(1 + \frac{\pi^2 a_i^2}{R_{0i}^2}\right)^{-1}, \tag{26}$$

where R_{0i} and a_i are taken as [38,39]

$$R_{0i} = 0.90106 + 0.10957A_i - 0.0013A_i^2 + 7.71458 \times 10^{-6}A_i^3 - 1.62164 \times 10^{-8}A_i^4, \tag{27}$$

$$a_i = 0.34175 + 0.01234A_i - 2.1864 \times 10^{-4}A_i^2 + 1.46388 \times 10^{-6}A_i^3 - 3.24263 \times 10^{-9}A_i^4. \tag{28}$$

This density distribution is shown as G1 in our study.

A.1.5 *Gupta density distribution* 2. This density distribution is in the same form as G1 density except for the values of R_{0i} and a_i given in the following forms [40]:

$$R_{0i} = 0.9543 + 0.0994A_i - 9.8851 \times 10^{-4}A_i^2 + 4.8399 \times 10^{-6}A_i^3 - 8.4366 \times 10^{-9}A_i^4, \tag{29}$$

$$a_i = 0.3719 + 0.0086A_i - 1.1898 \times 10^{-4}A_i^2 + 6.1678 \times 10^{-7}A_i^3 - 1.0721 \times 10^{-9}A_i^4. \tag{30}$$

This density is shown as G2 in our study.

A.1.6 *Wesolowski density distribution.* Wesolowski [41] has showed different parameters of 2pF density parametrised by [42]

$$\rho_0 = \frac{3}{4\pi R_0^3}\left(1 + \frac{\pi^2 a^2}{R_0^2}\right)^{-1}, \quad a = 0.39 \text{ fm}, \tag{31}$$

$$R_0 = R'\left[1 - \left(\frac{b}{R'}\right)^2 + \frac{1}{3}\left(\frac{b}{R'}\right)^6 + \cdots\right], \tag{32}$$

$$R' = \left[1.2 - \frac{0.96}{A^{1/3}}\left(\frac{N-Z}{A}\right)\right]A^{1/3}, \quad b = \frac{\pi}{\sqrt{3}}a. \tag{33}$$

This density is shown as W in our work.

A.1.7 *Schechter density distribution.* Schechter and Canto [43] have reported another parameters of 2pF density distribution shown by

$$\rho_0 = \frac{0.212}{1 + 2.66A^{-2/3}}, \quad R_0 = 1.04A^{1/3}, \quad a = 0.54 \text{ fm}. \tag{34}$$

This density is shown as S in our work.

A.1.8 *Moszkowski density distribution.* This density distribution proposed by Moszkowski [44] is in the form of 2pF density, and its parameters are given by

$$\rho_0 = 0.16 \text{ nucl./fm}^3, \quad R_0 = 1.15A^{1/3}, \quad a = 0.50 \text{ fm}. \tag{35}$$

This density is shown as M in our study.

A.1.9 *Density distribution of ^{58}Ni target nucleus.* In the calculations, the elastic scattering of ^{12}B projectile by ^{58}Ni has been investigated. For this purpose, the density distribution of ^{58}Ni target is obtained by

$$\rho(r) = \frac{\rho_0}{1 + \exp\left(\frac{r-c}{z}\right)}, \tag{36}$$

where $\rho_0 = 0.172$, $c = 4.094$ and $z = 0.54$ [45].

Appendix B: Nuclear potentials

B.1 *Proximity 1977 (Prox 77), Modified Proximity 1988 (Mod-Prox 88), Proximity 1995 (Prox 95), Proximity 2003 (Prox 2003), Proximity 2010 (Prox 2010) potentials*

Prox 77 version of proximity potential [46,47] is formulated as

$$V_N^{\text{Prox 77}}(r) = 4\pi\gamma b\bar{R}\Phi\left(\zeta = \frac{r - C_1 - C_2}{b}\right) \text{ MeV}, \tag{37}$$

where

$$\bar{R} = \frac{C_1C_2}{C_1 + C_2},$$
$$C_i = R_i\left[1 - \left(\frac{b}{R_i}\right)^2 + \cdots\right], \quad b \approx 1 \text{ fm}. \tag{38}$$

R_i, the effective radius, is given by

$$R_i = 1.28A_i^{1/3} - 0.76 + 0.8A_i^{-1/3}\text{fm}, \quad i = 1, 2. \tag{39}$$

γ, the surface energy coefficient, is given by

$$\gamma = \gamma_0\left[1 - k_s\left(\frac{N - Z}{N + Z}\right)^2\right]. \tag{40}$$

The universal function $\Phi(\zeta)$ is in the following form:

$$\Phi(\zeta) = \begin{cases} -\frac{1}{2}(\zeta - 2.54)^2 - 0.0852(\zeta - 2.54)^3, & \text{for } \zeta \le 1.2511, \\ -3.437\exp\left(-\frac{\zeta}{0.75}\right), & \text{for } \zeta \ge 1.2511. \end{cases}$$

Table 4. γ_0 and k_s values of Prox 77, Mod-Prox 88, Prox 95, Prox 2003-I, Prox 2003-II, Prox 2003-III and Prox 2010 potentials.

Potential type	γ_0 (MeV/fm^2)	k_s	Ref.
Prox 77	0.9517	1.7826	[48]
Mod-Prox 88	1.65	2.3	[49]
Prox 95	1.25284	2.345	[50]
Prox 2003-I	1.08948	1.9830	[51]
Prox 2003-II	0.9180	0.7546	[51]
Prox 2003-III	0.911445	2.2938	[51]
Prox 2010	1.460734	4.0	[47,52,53]

As a result of many studies on proximity potential, different values of γ_0 and k_s have been suggested although the other parameters of the potentials are the same as Prox 77. Each new situation has been evaluated as a different proximity potential. In this respect, seven various potentials are investigated in our study, and the γ_0 and k_s values of the potentials are listed in table 4.

B.2 *Broglia and Winther 1991 (BW 91) potential*

BW 91 potential [54] is taken as [55]

$$V_N^{\text{BW 91}}(r) = -\frac{V_0}{\left[1 + \exp\left(\frac{r-R_0}{a}\right)\right]}\text{MeV}, \tag{41}$$

where

$$V_0 = 16\pi\frac{R_1R_2}{R_1 + R_2}\gamma a, \quad a = 0.63 \text{ fm} \tag{42}$$

and

$$R_0 = R_1 + R_2 + 0.29,$$
$$R_i = 1.233A_i^{1/3} - 0.98A_i^{-1/3}, \quad i = 1, 2, \tag{43}$$

with γ as

$$\gamma = \gamma_0\left[1 - k_s\left(\frac{N_p - Z_p}{A_p}\right)\left(\frac{N_t - Z_t}{A_t}\right)\right],$$
$$\gamma_0 = 0.95 \text{ MeV/fm}^2, \; k_s = 1.8. \tag{44}$$

B.3 *Aage Winther (AW 95) potential*

AW 95 and BW 91 potentials are the same except for the following values [55,56]:

$$a = \left[\frac{1}{1.17(1+0.53(A_1^{-1/3}+A_2^{-1/3}))}\right] \text{fm} \quad (45)$$

and

$$R_0 = R_1 + R_2, \quad R_i = 1.2A_i^{1/3} - 0.09, \quad i = 1, 2. \quad (46)$$

B.4 *Bass 1980 (Bass 80) potential*

Bass 80 potential is formulated as [54,55]

$$V_N^{\text{Bass 80}}(s) = -\frac{R_1 R_2}{R_1 + R_2}\phi(s = r - R_1 - R_2) \text{ MeV}, \quad (47)$$

where

$$\phi(s) = \left[0.033 \exp\left(\frac{s}{3.5}\right) + 0.007 \exp\left(\frac{s}{0.65}\right)\right]^{-1} \quad (48)$$

and

$$R_i = R_s\left(1 - \frac{0.98}{R_s^2}\right),$$
$$R_s = 1.28A_i^{1/3} - 0.76 + 0.8A_i^{-1/3} \text{ fm}, \quad i = 1, 2. \quad (49)$$

B.5 *Christensen and Winther 1976 (CW 76) potential*

CW 76 potential [57] is given by [47]

$$V_N^{\text{CW 76}}(r) = -50\frac{R_1 R_2}{R_1 + R_2}\phi(r - R_1 - R_2) \text{ MeV}, \quad (50)$$

where

$$\phi(s) = \exp\left(-\frac{r - R_1 - R_2}{0.63}\right) \quad (51)$$

and

$$R_i = 1.233A_i^{1/3} - 0.978A_i^{-1/3} \text{ fm}, \quad i = 1, 2. \quad (52)$$

B.6 *Ngô 1980 (Ngo 80) potential*

Ngo 80 potential is written as [37]

$$V_N^{\text{Ngo 80}}(r) = \bar{R}\phi(r - C_1 - C_2) \text{ MeV}, \quad (53)$$
$$\bar{R} = \frac{C_1 C_2}{C_1 + C_2}, \quad C_i = R_i\left[1 - \left(\frac{b}{R_i}\right)^2 + \cdots\right], \quad (54)$$
$$R_i = \frac{NR_{ni} + ZR_{pi}}{A_i}, \quad i = 1, 2, \quad (55)$$
$$R_{pi} = r_{0pi}A_i^{1/3}, \quad R_{ni} = r_{0ni}A_i^{1/3}, \quad (56)$$
$$r_{0pi} = 1.128 \text{ fm}, \quad r_{0ni} = 1.1375 + 1.875 \times 10^{-4}A_i \text{ fm}. \quad (57)$$

The universal function $\phi(s = r - C_1 - C_2)$ (in MeV/fm) is taken as

$$\Phi(s) = \begin{cases} -33 + 5.4(s - s_0)^2, & \text{for } s < s_0, \\ -33 \exp[-\frac{1}{5}(s - s_0)^2], & \text{for } s \geq s_0, \\ s_0 = -1.6 \text{ fm}. \end{cases}$$

B.7 *Denisov (D) potential*

D potential is formulated by [55,58]

$$V_N^{\text{D}}(r) = -1.989843\frac{R_1 R_2}{R_1 + R_2}\phi(r - R_1 - R_2 - 2.65) \times \left[1 + 0.003525139\left(\frac{A_1}{A_2} + \frac{A_2}{A_1}\right)^{3/2} - 0.4113263(I_1 + I_2)\right] \text{MeV}, \quad (58)$$

where

$$I_i = \frac{N_i - Z_i}{A_i} \quad (59)$$

and

$$R_i = R_{ip}\left(1 - \frac{3.413817}{R_{ip}^2}\right) + 1.284589\left(I_i - \frac{0.4A_i}{A_i + 200}\right), \quad (60)$$
$$R_{ip} = 1.24A_i^{1/3}\left(1 + \frac{1.646}{A_i} - 0.191\left(\frac{A_i - 2Z_i}{A_i}\right)\right), \quad i = 1, 2. \quad (61)$$

$\phi(s = r - R_1 - R_2 - 2.65)$ is evaluated as

$$\phi(s) = \begin{cases} 1 - \frac{s}{0.7881663} + 1.229218s^2 - 0.2234277s^3 \\ -0.1038769s^4 - \frac{R_1 R_2}{R_1 + R_2}(0.1844935s^2 \\ +0.07570101s^3 + (I_1 + I_2)(0.04470645s^2 + \\ 0.0334687s^3)), \quad -5.65 \leq s \leq 0, \\ \left(1 - s^2\left(0.05410106\frac{R_1 R_2}{R_1 + R_2}\exp\left(-\frac{s}{1.76058}\right)\right.\right. \\ \left.\left. -0.539542(I_1 + I_2)\exp\left(-\frac{s}{2.424408}\right)\right)\right) \\ \exp\left(-\frac{s}{0.7881663}\right), \quad s \geq 0. \end{cases}$$

References

[1] M Thoennessen, *At. Data Nucl. Data Tables.* **98**, 43 (2012)
[2] S Leblond *et al*, *Phys. Rev. Lett.* **121**, 262502 (2018)
[3] https://www.nndc.bnl.gov/nudat2/chartNuc.jsp
[4] T Ohtsubo, Y Nakayama, T Izumikawa, S Takeda, N Nakamura, H Tanji and T Minamisono, *Hyperfine Interact.* **88**, 25 (1994)
[5] E O N Zevallos *et al*, *Phys. Rev. C* **99**, 064613 (2019)
[6] M Aygun, *Pramana – J. Phys.* **93**: 72 (2019)
[7] M Aygun, *Int. J. Mod. Phys. E* **27**, 1850055 (2018)
[8] M Aygun, *Commun. Theor. Phys.* **66**, 531 (2016)
[9] M Aygun, *Chin. J. Phys.* **53**, 080301 (2015)
[10] M Aygun and I Boztosun, *Few-Body Syst.* **55**, 203 (2014)
[11] M Aygun, *Ann. Nucl. Energy* **51**, 1 (2013)
[12] M Aygun, *Eur. Phys. J. A* **48**, 145 (2012)
[13] M Aygun, Y Kucuk, I Boztosun and A A Ibraheem, *Nucl. Phys. A* **848**, 245 (2010)
[14] A N Abdullah, *Pramana – J. Phys.* **89**: 43 (2017)
[15] M Freer, *Rep. Prog. Phys.* **70**, 2149 (2007)
[16] M Aygun, *Pramana – J. Phys.* **88**: 53 (2017)
[17] M Aygun and Z Aygun, *Nucl. Sci. Technol.* **28**, 86 (2017)
[18] M Aygun, *Rev. Mex. Fis.* **62**, 336 (2016)
[19] G R Satchler, *Direct nuclear reactions* (Oxford University Press, Oxford, 1983)
[20] I J Thompson, *Comput. Phys. Rep.* **7**, 167 (1988)
[21] M G Pellegriti *et al*, *J. Phys.: Conf. Ser.* **267**, 012011 (2011)
[22] P Descouvemont and I Baraffe, *Nucl. Phys. A* **514**, 66 (1990)
[23] G R Satchler and W G Love, *Phys. Rep.* **55**, 183 (1979)
[24] G D Alkhazov *et al*, *Nucl. Phys. A* **712**, 269 (2002)
[25] A V Dobrovolsky *et al*, *Nucl. Phys. A* **766**, 1 (2006)
[26] C W Glover, K W Kemper, L A Parks, F Petrovich and D P Stanley, *Nucl. Phys. A* **337**, 520 (1980)
[27] R A Rego, *Nucl. Phys. A* **581**, 119 (1995)
[28] A K Chaudhuri, *Phys. Rev. C* **49**, 1603 (1994)
[29] J X Li *et al*, *Chin. Phys. C* **34**, 452 (2010)
[30] C J Lin, Z H Liu, H Q Zhang, Y W Wu, F Yang and M Ruan, *Chin. Phys. Lett.* **18**, 1183 (2001)
[31] J Cook, *Commun. Comput. Phys.* **25**, 125 (1982)
[32] E O N Zevallos, *Investigation of elastic scattering of radioactive ^{12}B nucleus on ^{58}Ni target* (University of Sao Paulo, 2018)
[33] M El-Azab Farid, A A Ibraheem, J H Al-Zahrani, W R Al-Harbi and M A Hassanain, *J. Phys. G* **40**, 075108 (2013)
[34] L C Chamon *et al*, *Phys. Rev. C* **66**, 014610 (2002)
[35] W M Seif and H Mansour, *Int. J. Mod. Phys. E* **24**, 1550083 (2015)
[36] C Ngô, B Tamain, M Beiner, R J Lombard, D Mas and H H Deubler, *Nucl. Phys. A* **252**, 237 (1975)
[37] H Ngô and C Ngô, *Nucl. Phys. A* **348**, 140 (1980)
[38] R K Gupta, D Singh and W Greiner, *Phys. Rev. C* **75**, 024603 (2007)
[39] O N Ghodsi and F Torabi, *Phys. Rev. C* **92**, 064612 (2015)
[40] R K Gupta, D Singh, R Kumar and W Greiner, *J. Phys. G* **36**, 075104 (2009)
[41] E Wesolowski, *J. Phys. G* **11**, 1401 (1985)
[42] N K Dhiman, *Ukr. J. Phys.* **57**, 3 (2012)
[43] H Schechter and L F Canto, *Nucl. Phys. A* **315**, 470 (1979)
[44] S A Moszkowski, *Nucl. Phys. A* **309**, 273 (1978)
[45] M El-Azab Farid and M A Hassanain, *Nucl. Phys. A* **678**, 39 (2000)
[46] J Blocki, J Randrup, W J Swiatecki and C F Tsang, *Ann. Phys. (NY)* **105**, 427 (1977)
[47] I Dutt and R K Puri, *Phys. Rev. C* **81**, 064609 (2010)
[48] W D Myers and W J Swiatecki, *Nucl. Phys.* **81**, 1 (1966)
[49] R Kumar, *Phys. Rev. C* **84**, 044613 (2011)
[50] P Moller, J R Nix, W D Myers and W J Swiatecki, *At. Data Nucl. Data Tables* **59**, 185 (1995)
[51] K Pomorski and J Dudek, *Phys. Rev. C* **67**, 044316 (2003)
[52] I Dutt and R K Puri, *Phys. Rev. C* **81**, 047601 (2010)
[53] R Gharaei, V Zanganeh and N Wang, *Nucl. Phys. A* **979**, 237–250 (2018)
[54] W Reisdorf, *J. Phys. G* **20**, 1297 (1994)
[55] G L Zhang, Y J Yao, M F Guo, M Pan, G X Zhang and X X Liu, *Nucl. Phys. A* **951**, 86 (2016)
[56] A Winther, *Nucl. Phys. A* **594**, 203 (1995)
[57] P R Christensen and A Winther, *Phys. Lett. B* **65**, 19 (1976)
[58] V Yu Denisov, *Phys. Lett. B* **526**, 315 (2002)